Environmental Science Nano

ROYAL SOCIETY OF CHEMISTRY

PAPER

View Article Online
View Journal

Cite this: DOI: 10.1039/d1en00502b

Persistent arsenate–iron(III) oxyhydroxide–organic matter nanoaggregates observed in coal†

Yinfeng Zhang, [ab] Shehong Li, [b] Jing Sun, [b] Benjamin C. Bostick [c] and Yan Zheng *[de]

Received 2nd June 2021,
Accepted 12th August 2021

DOI: 10.1039/d1en00502b

rsc.li/es-nano

Understanding how natural nanoaggregates of iron (Fe) and organic matter (OM), currently identified in organic rich soil or peat, interact with metals and metalloids is environmentally significant. Coal is also organic-rich and exemplifies anoxic sedimentary environments with Fe usually as pyrite and not oxides. Here, we analyze the local structure of Fe (6880–21700 mg kg^{-1}) and As (45–5680 mg kg^{-1}) in representative Guizhou coal samples using X-ray absorption near-edge structure and extended X-ray absorption fine structure (XANES and EXAFS) to illustrate how Fe(III) and As(V) are preserved in coal formed from reduced, organic-rich precursors. Arsenic XANES indicates that >80% of As exists as As(V) with <14% of As associated with sulfides in 5 Guizhou coal samples, confirming published but unexplained results. An As–Fe shell at 3.25–3.29 Å in the As EXAFS suggests that this As(V) is adsorbed on Fe(III) oxyhydroxides as evidenced by Fe EXAFS in these coal samples. Significantly, lower Fe–Fe coordination numbers (CN) of 0.6–1.1 relative to those in 2-line ferrihydrite (CN = 1.6) and goethite (CN = 2.1) suggest that these Fe(III) oxyhydroxides are likely Fe–OM nanoaggregates protected by OM encapsulation and adsorption of arsenate. Such structurally stabilized composites of As(V)–Fe(III)–OM may be more widely distributed and allow oxidized As and Fe to persist in other organic-rich, reducing environments.

Environmental significance

The geochemical behavior of As is closely coupled with Fe minerals. Both are sensitive to redox processes. While laboratory studies have shown that natural organic matter (OM) regulates the transformation of Fe minerals and the associated As by forming stable, ternary complexes, studies in real reducing environments such as coal beds, marine and aquifer sediments are rare. This study demonstrates that oxidized As and Fe species persisted in reduced coal samples over a geological time scale. This is attributed to the structural protective effect of As(V)–Fe(III) oxides–OM nanoaggregates identified in coal samples based on spectroscopic evidence. The finding implies that such nanoscale mechanisms may be more prevalent in modern and ancient reducing environments.

1. Introduction

Recently, interest in natural nanoaggregates has grown due to their role in controlling the fate of inorganic pollutants in aqueous environments.[1–6] Natural nanoaggregates composed of iron (Fe) and organic matter (OM) have been observed in organic soils and organic soil horizons in wetlands, marine sediments, peatlands and permafrost.[7–11] Because metals and metalloids have strong affinities for Fe–OM nanoaggregrates,[11,12] mobilization in response to leaching of soil, thawing of permafrost,[8] and changes in redox conditions[13] has emerged as a transport pathway for pollutants to be reckoned with. Despite the growing environmental significance of Fe–OM nanoaggregates, our understanding of structural organization and complexation has relied primarily on a series of elegantly designed laboratory studies.[1,4–6,14–17] Molecular level characterization of Fe–OM nanoaggregates and their interaction with metals and metalloids in natural settings remains largely unexplored.

Coal is of interest because the precursor of coal is organic-rich peat,[10] with Fe–OM nanoaggregates identified in coal fly ash.[18]The global consumption of coal, a dirty fossil fuel, for

[a] Yunnan Key Laboratory of Plateau Wetland Conservation, Restoration and Ecological Services, College of Wetlands, Southwest Forestry University, Kunming, 650224, China
[b] State Key Lab of Environmental Geochemistry, Institute of Geochemistry, Chinese Academy of Sciences, Guiyang, 550081, China
[c] Lamont-Doherty Earth Observatory, Columbia University, 61 Route 9W, Palisades, NY 10964, USA
[d] State Environmental Protection Key Laboratory of Integrated Surface Water-Groundwater Pollution Control, School of Environmental Science and Engineering, Southern University of Science and Technology, Shenzhen, 518055, China
[e] Guangdong Provincial Key Laboratory of Soil and Groundwater Pollution Control, School of Environmental Science and Engineering, Southern University of Science and Technology, Shenzhen, 518055, China. E-mail: yan.zheng@sustech.edu.cn
† Electronic supplementary information (ESI) available. See DOI: 10.1039/d1en00502b

energy production has reached nearly 8 billion tons in 2016,[19] resulting in an array of environmental problems.[20] Coal exemplifies highly reduced, organic rich depositional environments that are also rich in toxic metals and metalloids.[21] It is an ideal natural system for investigating metals/metalloids and Fe–OM interactions, because the subsequent coalification processes that convert peat to coal result in a geological specimen rich in reduced elements, *e.g.*, carbon and sulfur, in thermodynamic disequilibrium of atmospheric oxygen. The prevailing paradigm about the redox state of metals like Fe and metalloids like As in coal is that much of the Fe and As in coal is bound with pyrite and/or other sulfides, indicative of the anoxic depositional environment during the initial stage of plant burial.[21–25]

At the same time, it is also recognized that As can be associated with organic-rich fractions of coal of widely variable sulfur content, suggesting that this is not a result of the enrichment of sulfur in organic-rich areas of the specimen.[26] Sequential leaching of low-S Wyoming coal[27] and coal from China,[28] England and Australia[29] points to this ubiquitous As–OM association but its nature is not well understood. For example, although small grains and veins of arsenopyrite and As-bearing pyrite have been identified by scanning electron microscopy in As-rich (up to 35 000 mg kg^{-1}) coal samples from Guizhou, China, the concentration of sulfidic As carrier-phases is inadequate to account for the As abundance on a whole coal basis, prompting investigators to propose iron oxides and iron phosphates as carrier-phases.[30] Further, the possibility that OM plays a role is evidenced by the spatially overlapping occurrence of As in Guizhou coal organic matter matrix (see Fig. 3 in Finkelman *et al.* 1999 (ref. 31)). Curiously, XANES analysis of 12 Guizhou coal samples has shown the dominance of oxidized As(v), ranging from 75% to 100%.[32,33] Yet, how and why coal samples contain reduced minerals such as pyrite and at the same time As(v) and possibly Fe(iii) oxides remain unexplained.

We hypothesize that Fe(iii) and As(v) may occur in coal by the formation of As–Fe–OM complexes that involve Fe–OM nanoaggregates to provide a structural protection mechanism against reduction in an anoxic depositional environment, with the stability of Fe–OM nanoaggregates enhanced by sorption of arsenate. Our hypothesis stems from growing spectroscopic and structural evidence demonstrating that polyvalent cations such as Fe can connect As and OM and form stable complexes.[14,15,34] In these ternary systems, OM complexation and micellar protection decrease the reactivity of Fe(iii) oxyhydroxides, analogous to the stabilization of Fe(iii) in ferritin proteins. Arsenate, and potentially phosphate retention on these Fe colloids and small sized aggregates, may also help to stabilize them.[35]

To test our hypothesis, a suite of freshly collected Guizhou coal samples from the same high-As coal formation previously investigated[32,36] and found to contain oxidized As(v)[36] are analyzed for their chemical and bulk mineralogical compositions. Five coal samples, representative of high-As Guizhou coal, together with As–Fe–OM aqueous solutions, and As and Fe compounds and minerals taken as standard reference minerals, are subjected to synchrotron analysis. The speciation and local coordination environments of As and Fe are characterized by XANES and EXAFS,[14,15,34] with data reduction involving shell-fitting or least-squares linear combination fitting through an iterative process. The results suggest that our hypothesis is viable for coal, with implications on the mobility of Fe and As in organic-rich, reducing sedimentary aquifers discussed at last.

2. Materials and methods

2.1 Coal samples

Most of the coal in the world was deposited in the late Paleozoic (410 to 245 million years before the present) during time periods when global productivity was high in tropical, flooded anoxic environments where plant organic matter was best preserved.[37] Based on prior studies,[36] coal samples from the late Permian (299 to 251 million years before the present) Longtan Formation in the Guizhou Province[36] of southwest China (Fig. S1†) are chosen for sampling. The Longtan Formation consists of limestone-bearing anthracite (indicative of the highest coalification temperature and pressure) coal beds in the Anlong County (samples C1, C2, C3 and C5) and Xingren County (sample C4), Guizhou (Fig. S1†). These anthracite coal samples rich in limestone also contain extensive Carlin-type gold deposits rich in As, Hg, Sb and Tl.[36] All coal samples were collected in polyethylene zip-lock bags and covered with aluminum foil immediately in the field in July 2014. Upon returning to the laboratory on the same day, the samples were refrigerated at 4 °C until analysis also in July 2014. The coal storage method followed the established practice of coal geologists and geochemists[33,38–40] (see details in SM1 and Table S1†).

2.2 Bulk chemical and mineralogical analyses

Aliquots of the coal samples were air dried for analysis. The concentrations of C and S were determined on an elemental analyzer (Elementar, vario MACRO, Germany) as follows: 0.3000 ± 0.0005 g of samples were weighed and wrapped with tin foil and then heated to up to 1200 °C for analysis, with a precision of ~0.5%. The concentrations of Fe and As were determined in total acid digests by inductively coupled plasma-optical emission spectroscopy (ICP-OES, Thermo 6000) and hydride-generation atomic fluorescence spectroscopy (HG-AFS, AFS-2100e), respectively. The acid digestion using high-pressure canisters followed an established protocol from the State Key Laboratory of Environmental Geochemistry (SKLEG), Institute of Geochemistry of Chinese Academy of Sciences.[41] Briefly, 3 mL of concentrated HNO_3 (trace metal grade) and 1 mL of concentrated $HClO_4$ (trace metal grade) were added to 0.0500 ± 0.0003 g of solids in Teflon bottles, and placed in an oven at 160 °C for 24 h or longer until the digest became clear. The digested samples were then heated on a hot plate to near

dryness and redissolved with 1% HNO_3. Two standard reference materials (SRMs), GSS14 (standard soil sample, Fe = 37 240 ± 420 mg kg^{-1}, As = 6.5 ± 1.3 mg kg^{-1}) and GSS16 (standard soil sample, Fe = 31 360 ± 350 mg kg^{-1}, As = 18 ± 2 mg kg^{-1}), were simultaneously digested and analyzed for quality control and assurance, with data within 90–110% of certified values. Bulk mineralogy was analyzed through X-ray diffraction analysis (XRD, D/Max-2200) using a protocol previously described.[42]

2.3 X-ray absorption spectroscopy

2.3.1 Standard reference materials (SRMs)

As mineral SRMs. Arsenopyrite (FeAsS, As oxidation state As^0), realgar (AsS), orpiment (As_2S_3, As oxidation state As^{3+}), sodium arsenite ($NaAsO_2$, Sigma-Aldrich, >99%), sodium arsenate heptahydrate ($Na_2HAsO_4{\cdot}6H_2O$, Sigma-Aldrich, 99.995%) and scorodite ($FeAsO_4{\cdot}2H_2O$) were obtained from the Certified Reference Material Center, China, with their identities confirmed by XRD analysis.

Sorbed As(v) samples as SRMs. These were prepared by adding small aliquots of As(v) solutions to a variety of inorganic mineral compounds including 2-line ferrihydrite and goethite (listed in Table S2†) acting as inorganic adsorbents (2 g L^{-1} suspension density) to reach an initial spiked As concentration of 100 mg kg^{-1}, with the final pH adjusted to be between 7.0 and 7.5, with details published previously.[41] The spectra of these sorbed As(v)-SRMs were collected at the Beijing Synchrotron Radiation Facility (BSRF) in 2013, with details available in a prior study[41] for the least-squares linear combination fitting (LCF) in this study. The modified method of Schwertmann and Cornell[43] is used to synthesize 2-line ferrihydrite and goethite with details described in the ESI† (SM2).

As(v)–OM and As(v)–Fe(III)–OM complexes as SRMs. These complexes are prepared using the method of Mikutta *et al.*[14] with modifications, with details in the ESI† (SM3). Standard reference materials humic acid (HA, Suwannee River humic acid standard II) and fulvic acid (FA, Suwannee River fulvic acid standard) were purchased from the International Humic Substances Society (IHSS). Briefly, aqueous solutions of As(v) were added to HA or FA to prepare As(v)–HA or As(v)–FA complexes. Similarly, As(v) & Fe(III) solutions were simultaneously added to HA or FA to prepare As(v)–Fe(III)–HA or As(v)–Fe(III)–FA complexes. The final working standards contained 0.05 mg As per mL and 4 mg HA or FA per mL, with or without 0.2 mg Fe per mL.

Among the SRMs, As complexed to organic matter, either humic or fulvic acid (As–HA and As–FA, collectively As–HA/FA), and As and Fe bound to either humic or fulvic acid (As–Fe–HA and As–Fe–FA, collectively As–Fe–HA/FA) are the most significant to the coal samples in this study.

2.3.2 Spectra collection. X-ray absorption spectroscopy (XAS) spectra of the 5 coal samples were collected on beamline 1W1B at BSRF in July 2014. The spectra of C1 and C3 were collected again on beamline 4-1 at the Stanford Synchrotron Radiation Lightsource (SSRL) for inter-laboratory comparison in January 2019 and were found to be nearly identical to those collected in July 2014 at BSRF (Fig. S2†). The BSRF ring current was 200 mA and the energy was 2.5 GeV, while the SSRL operates at 500 mA and 3 GeV. Both beamlines used Si(220) monochromators with an angle of incident ray or phi angle of 90°, and were detuned 50% to decrease higher-order harmonics and prevent detector saturation. XAS spectra were collected at around the arsenic and iron K-edges, respectively, from −200 to 1000 eV (leading to a k range from 0 to 13 $Å^{-1}$).

Iron spectra were collected using Soller slits and a Mn filter. Fe spectra were calibrated internally using Fe foil between the second and third ionization chambers (with an inflection point at 7112.0 eV). Arsenic spectra were calibrated with scorodite (with its edge at 11 874.1 eV). The coal and reference materials were analyzed in fluorescence mode using a Lytle detector at BSRF or a 31-element Ge detector at SSRL. Powdered reference minerals were analyzed in transmission mode. Sample thicknesses were determined based on the quantity of mineral needed to achieve an absorption of 1 μx (37% of light transmitted at the edge, about 10–20 mg over an area of a few cm^2). At least three scans were obtained for each sample/reference. No evidence of photooxidation or reduction was observed in successive scans of any coal, or in the reference compounds, under these analytical conditions.

2.3.3 Data reduction. X-ray absorption near edge structure (XANES) and extended X-ray absorption fine structure (EXAFS) spectra were processed using the ATHENA software. For each sample/reference, several collected scans were merged into one, and normalized with linear pre-edge and quadratic post-edge functions and converted to a k^3-weighted chi function as needed. The normalized spectra were then used for either LCF or shell-fitting following methods in our prior studies.[44,45]

Briefly, LCFs were performed on: (1) As XANES spectra to determine the oxidation state of As in the Guizhou coal samples; (2) As EXAFS spectra to determine how As is retained in these coal samples. For part (1), As XANES LCFs were attempted for energies ranging from −20 to 35 eV using different combinations of arsenopyrite, orpiment, sodium arsenite and scorodite as SRMs (combinations listed in Table S2†). For part (2), LCFs were performed over a k-range of 2–12 $Å^{-1}$ using As(v)–Fe–HA/FA SRMs, sorbed As(v) on inorganic mineral SRMs, and As-bearing sulphides (combinations listed in Table S2†). For each LCF, different combinations of SRMs were all considered in fitting until the best fits were achieved (Fig. 1 and S3; Tables 1, S2 and S6†). The estimated fit errors of the LCF methods are calculated with ATHENA and based on spectral quality, fit quality and similarity between reference spectra, and were typically <5% for each component.

Shell fitting was performed using ATHENA and WinXAS on both Fe and As EXAFS spectra to determine their coordination environments.[46,47] This approach used k^3-weighted EXAFS spectra over a k-range of 2–12 $Å^{-1}$ and fitted

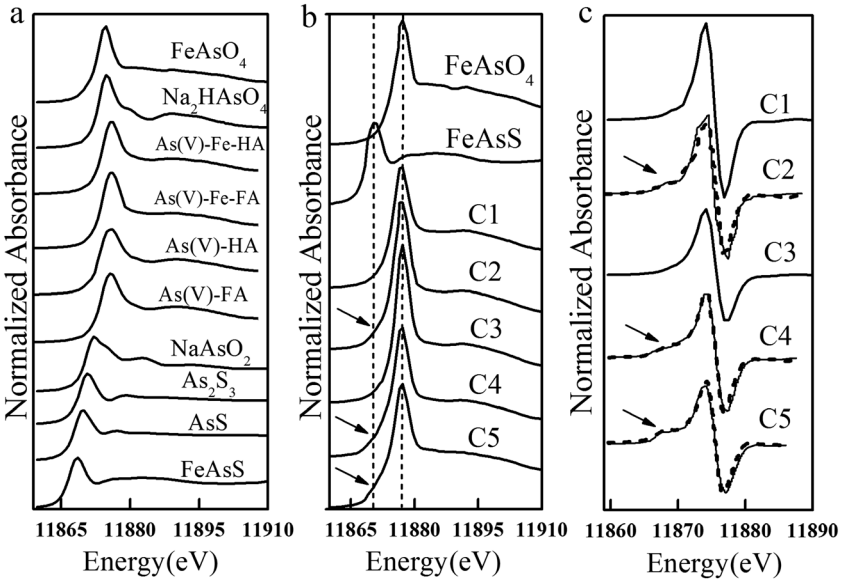

Fig. 1 XANES spectra of the (a) compounds used as As standards and synthetic As–Org (HA/FA) and As–Fe–Org (HA/FA) standards and (b) 5 coal samples with 2 standard As compounds ($FeAsO_4$(v), FeAsS(0)) that share the same position of absorption edge as that of the samples, and (c) linear combination fits (dashed lines) for coal samples (C2, C4, C5) in the first-derivative of XANES (Table 1). Coal samples C1 and C3 (fits not shown) are 100% As(v) (Table 1).

in both *R*-space and *k*-space. Local structures were determined by varying the coordination number (CN), distance (*R*, in Å), and disorder as estimated by the Debye–Waller factor (σ^2) for each shell. The coordinating atom (Z) for each shell is inferred based on their unique phase shift and amplitude functions, which are accurately calculated for different atom-pairs that were calculated using the FEFF 7 code. During fitting, E_0 shifts were correlated between the first and second shells and $S_0{}^2$ was fixed to 0.9 for both As and Fe. The other parameters (*R*, CN, σ^2) were free to change but constrained to positive values.

The number of Fe atoms in body-centered cubic iron clusters is calculated by eqn (1) below. We also calculated the *n* values for the coal samples and SRMs based on the CNs determined from Fe EXAFS using also eqn (1), under the assumption that the Fe clusters in the coal samples and SRMs are also body-centered cubic.

$$\mathrm{CN} = \frac{8\times 1 + (\sqrt[3]{n}-1)\times 2 + (\sqrt[3]{n}-1)^2\times 3 + (\sqrt[3]{n}-1)^3\times 6}{(\sqrt[3]{n}+1)^3} \quad (1)$$

3. Results and discussion

3.1 Samples selected to represent Permian high-As Guizhou coal

Five coal samples were selected for XAS analysis on the basis of their similarities in compositions to a larger group of 24 coal samples collected from Guizhou in this and prior studies[32,36] (Table S3†). The As, Fe and S concentrations in the 5 coal samples ranged from 45 to 5676 mg kg^{-1}, 0.6 to 2.1%, and 1.3 to 2.8%, respectively (Table 1). The concentrations of As in coal vary widely worldwide, with a frequently cited range being between 7 and 4000 mg kg^{-1}.[29] The sample with the highest As concentration, C4 from Xingren, contained the lowest Fe concentration. No significant correlations between the concentrations of As–Fe, As–S and Fe–S are evident among the larger group of coal samples (Table S3†).

Likewise, the bulk mineralogy determined by XRD was also similar between the 5 coal samples investigated and the larger group (Tables 1 and S4†). The pyrite content ranged from 2% to 7% in the 5 coal samples (Table 1), while being 1% to 13% in all 24 coal samples (Table S4†). X-ray absorption spectroscopy (XAS) and scanning electron microscopy with energy dispersive X-ray spectroscopy (SEM-EDX) have shown that the most common As species in Cretaceous (145.5 and 65.5 million years before the present) coal samples from Kentucky, Wyoming and Idaho in the USA was pyritic arsenic.[33,40,48] In addition to pyrite, other sulfide minerals including chalcopyrite, sphalerite, orpiment and realgar have also been identified as As-bearing phases in coal samples from Australia and the US.[49] However, unlike most coal samples in which sulfidic minerals account for most of the As occurrence, it has been demonstrated that pyrite is insufficient to account for the abundant As in Guizhou coal samples.[30,31,36]

3.2 Arsenic XANES spectra of the Guizhou coal samples confirm oxidized arsenic

It has been shown that approximately 75% to 100% of As is As(v) in the As K-edge absorption edge of 6 Guizhou coal samples containing 203 to 32 300 mg kg^{-1} As (see Fig. 1 in Ding *et al.* 1999 (ref. 32)). The XANES spectra of the 5 coal

Table 1 Bulk minerology, concentrations of Fe, C, S and As, and speciation of As in five Guizhou coal samples from China

	Chemical and mineral compositions							Arsenic species				
Sample	Fe (mg kg^{-1}, ICPOES)	C (%, elemental analyser)	S (%, elemental analyser)	Ill. (%, XRD)	Kao. (%, XRD)	Hem. (%, XRD)	Py. (%, XRD)	$As_{(Total)}$ (mg kg^{-1}, HG-AFS)	As(v)(%)	As(III) (%)	As–sulfide (%)	*R*-factor[a]
ML-1(C1)	10 928	60.2	1.6	28	12	2	4	5676	100[c]	—	—	—
JL-92(C2)	7859	76.2	2.8	24	26	2	7	175	85 ± 5[b]	9±6[b]	6 ± 5[b]	0.006
LC-1(C3)	15 480	64.5	1.7	17	23	n.d[a]	2	698	100[c]	—	—	—
GCQ-5(C4)	21 733	56.7	1.9	18	15	4	4	45	86 ± 4 [b]	2 ± 3[b]	12 ± 4[b]	0.004
Hz-Au-97(C5)	6885	66.2	1.3	23	22	<1	2	111	81 ± 5 [b]	5 ± 4[b]	14 ± 5[b]	0.005

[a] *R*-factor represents the relative error of the fit and data. [b] Calculated from LCF of XANES. [c] There is only one peak at the position of As(v) in XANES for C1 and C3 (Fig. 1), 100% As(v) is assumed.

samples examined here are also indicative of a predominantly As(v) mode based on their edge positions of 11 874.3 eV (Fig. 1b), confirming the earlier, though unexplained, results in Ding *et al.* 1999.[32] The XANES peak of As shifts towards a higher energy level with increasing oxidation state of As in the SRMs, from 11 867 eV for nominally zero valent As (as in FeAsS) to 11 871.5 eV for As(III) as in $NaAsO_2$ and 11 874.0 eV for As(v) as in $FeAsO_4$ (Fig. 1a).

The majority of As (>80%) is present as As(v) in coal samples C2, C4, and C5 based on LCF analysis of their respective As XANES spectra (Table 1). The As XANES spectra of samples C2, C4 and C5 also contain a feature at ~11 868 eV that is easier to tell in the first derivative spectra (Fig. 1c) than in the XANES (Fig. 1b), indicative of a small fraction (<20%) of pyritic As or FeAsS (Table 1). Due to the absence of any other peaks in C1 and C3 (Fig. 1b and c), nearly 100% of As are taken as As(v) without LCF analysis (Table 1). Arsenic EXAFS also supports As–O bonds with lengths consistent with As(v) and thereby further confirms the dominance of As(v) in the Guizhou high-As coal samples (Fig. 2).

We are confident that the prevalence of this As(v) is an accurate representation of the Guizhou coal samples because the samples contained no evidence of oxidation before or after analysis, and the XANES spectra of C1 and C3 collected in Beijing in 2014 and at Stanford in 2019 are nearly identical (Fig. S2†). Coal samples selected for inclusion in this study were based on their lack of any obvious signs of physical or chemical alterations. The reduced pyrite phases are stable, and As in other coal samples prepared the same way is typically not oxidized.[32,36]

3.3 Iron and arsenic local structures in the As–Fe–OM standards

A handful of papers have examined Fe and As local structures by shell fitting of Fe and As EXAFS of ferrihydrite, goethite, and scorodite to compare with that of As–Fe–OM SRMs (Table S5†). The most relevant is the As–Fe–OM standard, and our shell fitting results of the As–Fe–HA/FA SRMs (Table 2) are consistent with those of Mikutta *et al.*[14] (Table S5†). All As–FA/HA and As–Fe–HA/FA SRMs have similar first As–O coordination shells at a distance of 1.70–1.71 Å as expected for arsenate; this is consistent with the K-edge absorption edges of synthetic As(v)–Fe–OM SRMs of As(v)–Fe–HA/FA and As(v)–HA/FA at 11 874.0 eV (Fig. 1a).

The Fe EXAFS K-edge spectra of the As–Fe–HA and As–Fe–FA standards are nearly identical (Fig. 3). Each contains 2 shells, an Fe–O shell near 1.95 Å and an Fe–Fe shell at ~3.03 Å (Fig. 3b). The presence of an Fe–Fe shell is a key indication that Fe atoms are likely in oxyhydroxide clusters within the organic matter. Furthermore, the CN_{Fe-Fe} of the Fe–Fe shell decreases from 2.1 to 1.6 to 1.3 for goethite, ferrihydrite and the As–Fe–HA SRM, respectively, corresponding to also the estimated decreasing number of Fe atoms (n) as body-centered cubic clusters from 130 to 60 to 38 (Table 2).

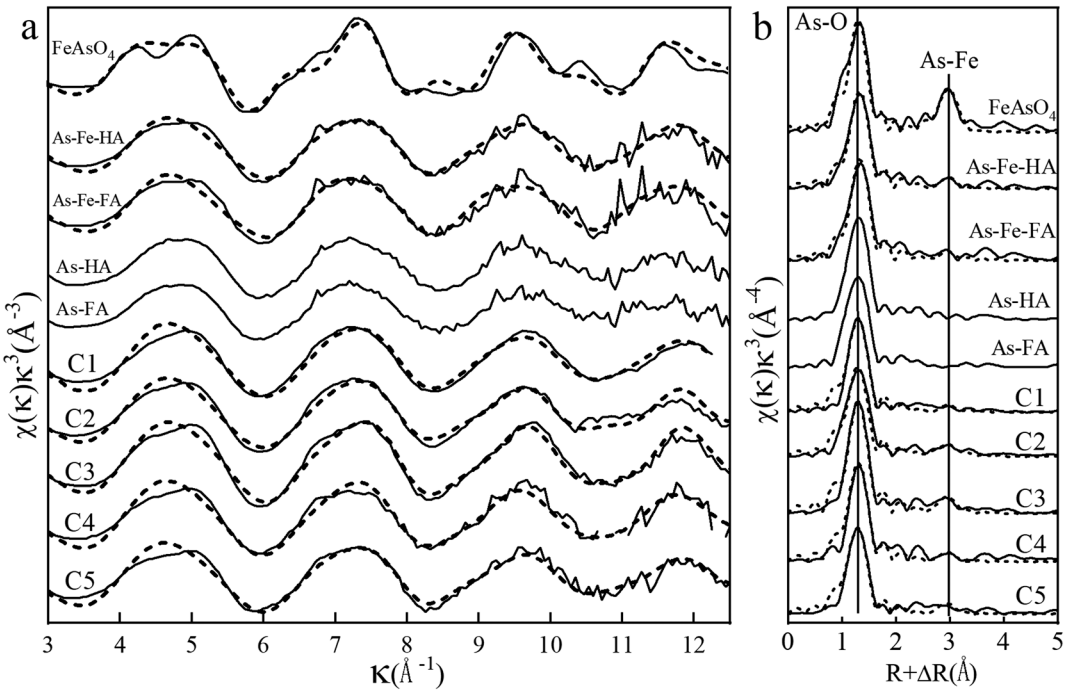

Fig. 2 Arsenic K-edge EXAFS spectra with (a) k^3-weighted fitting in k-space for the five coal samples and As–Fe–HA/FA standards and (b) peak fits for the coal samples and As–Fe–HA/FA standards in R-space. As–Fe shells are absent in standards of As–HA/FA (fits not shown). Solid lines represent data, and dashed lines represent As–O and As–Fe path fitting results (Table 2).

The similarity between the As K-edge EXAFS spectra of As–Fe–HA and As–Fe–FA (Fig. 2) allows us to use just one of them (As–Fe–HA, Table S2†) as the SRM for LCF in order to characterize the As structure in the coal samples (Table S2†). Furthermore, the As–Fe shells at ~3.29 Å are also evident in both As–Fe–HA and As–Fe–FA standards (Fig. 2b). The coordination numbers for these As–Fe shells are about 0.7 (Table 2), consistent again with the characterization of similar As–Fe–OM ternary complexes (Table S5†) by Mikutta *et al.*[14]

Table 2 Arsenic and Fe local structures for selected model compounds and coal samples

		Path	CN[a]	R^b	σ^{2c}	Path	CN[a]	Number of Fe atoms[d]	R^b	$\Delta E_0{}^g$ (Ev)	σ^{2c}
As K-edge											
Model compounds	$FeAsO_4{\cdot}2H_2O$	As–O	4.0	1.69	0.002	As–Fe	4.1	—	3.30	1.58	0.006
	As(v)–Fe–HA	As–O	3.7	1.70	0.002	As–Fe	0.7	—	3.29	5.54	0.003
	As(v)–Fe–FA	As–O	3.8	1.71	0.002	As–Fe	0.7	—	3.29	5.19	0.005
	As(v)–HA	As–O	3.8	1.69	0.002	As–Fe	—[e]	—	—[e]	—	—[e]
	As(v)–FA	As–O	3.8	1.69	0.002	As–Fe	—[e]	—	—[e]	—	—[e]
Coal samples	C1	As–O	3.9	1.69	0.003	As–Fe	0.7	—	3.27	6.58	0.004
	C2	As–O	3.8	1.69	0.003	As–Fe	0.7	—	3.29	6.57	0.002
	C3	As–O	4.0	1.68	0.002	As–Fe	0.8	—	3.28	5.62	0.003
	C4	As–O	3.9	1.69	0.004	As–Fe	0.7	—	3.28	5.86	0.005
	C5	As–O	4.0	1.69	0.002	As–Fe	0.8	—	3.26	4.32	0.006
Iron K-edge											
Model compounds	Goethite	Fe–O	3.0	1.98	0.005	Fe–Fe	2.1	130	3.03	3.71	0.005
	Ferrihydrite	Fe–O	3.1	1.98	0.005	Fe–Fe	1.6	60	3.03	3.62	0.009
	As–Fe–HA	Fe–O	4.5	1.98	0.008	Fe–Fe	1.3	38	3.04	2.65	0.007
Coal samples	C1	Fe–O	5.1	1.99	0.006	Fe–Fe	0.6	6	3.03	3.54	0.006
	C2	Fe–O	5.3	1.99	0.006	Fe–Fe	0.7	8	3.05	2.89	0.003
	C3	Fe–O	5.2	1.99	0.005	Fe–Fe	1.0	21	3.05	3.46	0.005
	C4[f]	—	—	—	—	—	—	—	—	—	—
	C5	Fe–O	5.3	1.98	0.008	Fe–Fe	1.1	25	3.04	3.30	0.004

[a] Coordination number. [b] Path length (Å), the accuracy of the interatomic distance R is within 0.01 Å,. [c] Debye–Waller parameter. [d] The numbers of Fe atoms are calculated based on CNs of Fe–Fe shells (Fig. 4, calculation method is provided in Materials and methods). [e] The "As–Fe" shell is either absent or undetectable at certain coordination numbers in the As–HA/FA standards. [f] Iron structure in C4 is like that of pyrite (Fig. 3b); the Fe–Fe shell is not obvious. [g] Energy shift parameter.

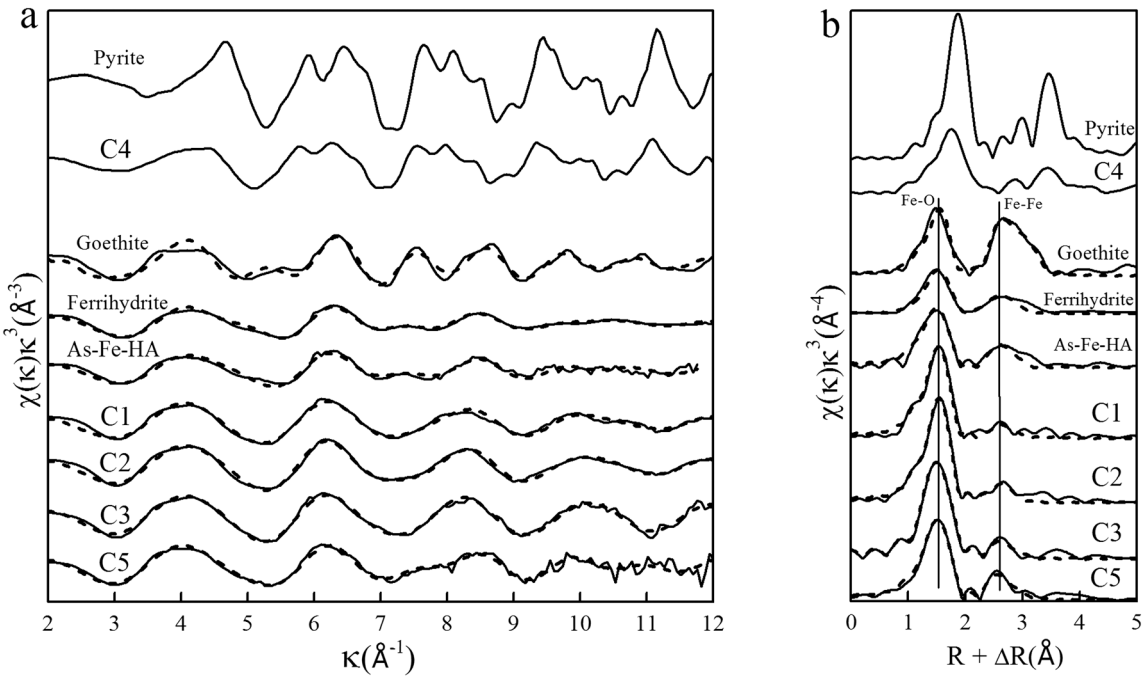

Fig. 3 Iron K-edge EXAFS spectra with (a) k^3-weighted fitting in k-space for the coal samples (C1, C2, C3, C5) and three standards (goethite, ferrihydrite and As–Fe–HA), sample C4 and pyrite; (b) peak fits in R-space for the coal samples (C1, C2, C3, C5) and three standards (goethite, ferrihydrite and As–Fe–HA), sample C4 and pyrite. Solid lines represent data, and dashed lines represent Fe–O and Fe–Fe path fitting results (Table 2).

3.4 EXAFS spectra of arsenic in the Guizhou coal samples suggest interactions with Fe–OM

The As EXAFS spectra of the Guizhou coal samples exhibit similarities to those of $FeAsO_4$ and As–Fe–OM (HA/FA) and are dominated by two shells, an As–O shell and an As–Fe shell (Fig. 2). The As–O bond length is 1.68–1.69 Å and is typical for As(v)–O bonds (Table 2), and is much shorter than As(III)–O bonds (1.77 Å).[50] The second-shell of As EXAFS is more informative in terms of how As is retained in these coal samples. These As(v)-rich coal samples contain a clear but small As–Fe shell at about 3.28 Å, similar to the distances observed for edge-sharing polyhedra for As adsorbed on Fe oxides.[51]

The coordination number of 0.7–0.8 for the As–Fe shell in the coal samples is also consistent with that for As complexation to iron. This is because these CN_{As-Fe} values are much lower than that of scorodite $FeAsO_4{\cdot}2H_2O$ (CN_{As-Fe} = 4), but are nearly identical to the coordination numbers determined for the synthetic As–Fe–FA and As–Fe–HA complexes used as SRMs (CN_{As-Fe} = 0.7, Fig. 2b, Table 2). This similarity suggests that As(v) in these coal samples is also bound to organic matter through bridging to one or more Fe atoms, with further Fe EXAFS evidence described in section 3.5, and not directly complexed by organic matter.

Aside from the shell fitting results above, linear combination fitting, which depends on considering a complete and accurate set of SRM spectra (Table S2†), provides information about the relative fraction of each SRM in the samples.[52] It is worth noting that the As EXAFS spectra of the coal samples were best reproduced with combinations of spectra of the As–Fe–HA and As–HA complexes as SRMs; using only As adsorbed on inorganic minerals or only As–sulfur minerals as standards, the fits are very poor (Fig. S3, Table S6†). Because the combination of As–Fe–HA and As–HA spectra could consistently describe the As EXAFS spectra of all coal samples, without any adsorbed As on inorganic minerals or As-bearing sulfides, this implies that these soluble ternary complexes are effective models of the stable As(v)–Fe(III)–OM local structures in coal samples (Table S6†).

3.5 EXAFS spectra of iron in the Guizhou coal samples suggest small sized Fe particles

Iron K-edge EXAFS complements the information on the As coordination environment inferred from As EXAFS and allows for a more complete characterization of the structure of the As–Fe–OM ternary complexes in these coal samples. Except for pyritic-Fe in C4, the Fe in the four other coals was primarily Fe(III) and had local structures similar to those of ferrihydrite and/or goethite (Fig. 3), with interaction with OM further modifying its structure. In these Fe(III)-rich spectra, the first shell observed was attributed to 4–5 oxygen atoms coordinated to Fe at a distance of 1.98–1.99 Å (Fe–O in Fig. 3 and Table 2). This distance is similar to those of our As–Fe–HA/FA references (and Fe(III) oxyhydroxides with octahedral Fe).[34,53] The second shell observed was an Fe–Fe shell (edge sharing Fe) at a distance of around 3.03 Å, identical to that of ferrihydrite and goethite.

Unlike many other coal samples containing abundant pyrite,[54–56] pyrite was evident only in C4 from Xingren whereas C1, C2, C3 and C5 from Anlong all show abundant Fe(III) oxyhydroxides (Fig. 3). The Fe EXAFS spectrum of C4 contains the same shells with pyrite (Fe–S for example at 2.2 Å, and a series of longer Fe–Fe and Fe–S shells) but with lower intensities, suggesting that there was an additional component or components that were difficult to isolate. Accordingly, the results also indicate that Fe exists as a pyrite-like phase in coal C4, while much smaller quantities of pyrite are present in the other samples (Table 1), interpreted as representing a new mode of Fe occurrence as discussed below.

The CNs of Fe–Fe shells in four coal samples (C1, C2, C3, C5) range from 0.6 to 1.1 (Table 2), significantly smaller than that of the As–Fe–HA reference (CN_{Fe-Fe} 1.3), 2-line ferrihydrite (CN_{Fe-Fe} 1.6) and goethite (CN_{Fe-Fe} 2.1). Significant to this study, the CNs are dependent on particle size because small particles have a significant fraction of atoms on surfaces and edges relative to fully coordinated crystallographic sites, and also experience distortion in the crystal that increases disorder.[34] Thus, this small coordination number indicates that the Fe polymers bound within OM in the coal samples have a smaller particle size or similar particle size to those of the As–Fe–HA/FA reference, and must be smaller than even nanoparticles like 2-line ferrihydrite. To evaluate how small these Fe particles can be in coal samples, we calculate how many Fe atoms are required to achieve such small CNs. Based on the observed Fe–Fe coordination numbers in coal samples, the Fe(III) oxyhydroxide nanoparticles in these 4 coal samples contain only 6 to 25 Fe atoms (Table 2), suggesting that they are smaller than those of 2-line ferrihydrite (Fig. 4 left panel). The diameters of naturally occurring ferrihydrite particles have been estimated to be 2.4–2.9 nm,[57] supporting our hypothesis of Fe(III)–OM nanoaggregates.

It has also been shown that interaction between Fe and OM occurs when the ratio of C/(C + Fe) is above 0.89 in laboratory synthesized DOM/Fe coprecipitates.[16] The ratios of C/(C + Fe) of coal samples are above 0.9. In addition, we have calculated the site saturation based on crystal limitations (the number of hydroxyl species present on the surface of iron hydroxides). Based on the number of Fe atoms calculated from the CNs of the Fe–Fe shell and the As/Fe ratio in the 4 Guizhou/Anlong coal samples, C1, C2, C3 and C5, all plot at the bottom of the line of the theoretically estimated Fe atoms and CN using eqn (1) (Fig. 4 right panel). This suggests that the As atoms in these four coal samples are not enough to cover the surfaces of Fe(III) hydroxides, which implies that surface sites are also available for organic complexation, supporting our hypothesis of stabilization of As(V)–Fe(III)–OM nanoaggregates.

3.6 Structural protection by As(V)–Fe(III)–OM nanoaggregates

The mechanism responsible for oxidized As(V) in Guizhou coal samples containing pyrite has remained enigmatic since its discovery more than two decades ago.[36] Our spectroscopic characterization of the Guizhou coal samples leaves little doubt that both Fe(III) and As(V) are stabilized within these coal samples, likely as As(V)–Fe(III)–OM nanoaggregates. A ternary complex of As(V) bound through edge-sharing with small (<2.4 nm) Fe(III) oxyhydroxide nanoparticles within the organic matter matrix is reasoned to offer the structural protection against reduction in the wetland or peatland anoxic environments encountered by these precursors of coal. XAS analysis of eight peat profiles (As 3–1800 mg kg^{-1}, Fe 90–600 mmol kg^{-1}, S 10–680 mmol kg^{-1}) collected from suboxic to reducing environments revealed large amounts of ferric species, or about 42–80% of Fe, which is attributed to stabilization by Fe(III)–NOM complexes.[58]

Complexation of organic matter and with As(V) may be a driving force in reducing the particle size of Fe(III)–OM nanoaggregates within coal. Organic matter is able to change the surface charge density of iron oxides/hydroxides, and therefore affect the aggregation of iron minerals.[5,35] Recent lab studies based on XAS, X-ray photoelectron spectroscopy and infrared spectroscopy have demonstrated that the presence of citrate and As(V) decreases the size of ferrihydrite particles, with reductions in Fe CNs of up to 28%.[59,60] These studies have further confirmed that it is the position of

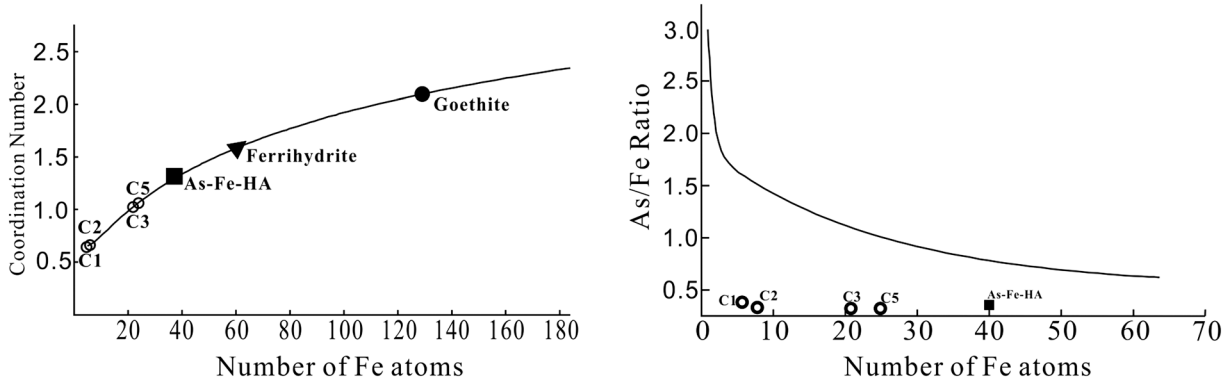

Fig. 4 Theoretically calculated coordination numbers (CNs) of Fe–Fe shell increases with the increase of Fe atoms in an iron cluster (based on Inskeep *et al.*[69]). The hollow circles (4 Guizhou coal samples) show the CNs determined by Fe EXAFS (left) and the molar ratios of As/Fe (right).

phenol groups, rather than the number of phenol groups, that controls the interaction between Fe and organic matter, and, in turn, triggers the decrease of CNs of the Fe–Fe shell.[60] Other lab studies have also revealed that the interactions between organic ligands like carboxyl groups in dissolved organic matter (DOM) and Fe(III) favor the formation of Fe minerals with smaller sizes and thus smaller CNs.[16,34] Taken together, these recent lab studies suggest the possibility that natural organic matter may provide protection from Fe(III) reduction during coalification.

Given the long geological time scale for coal formation, the stability of these As(V)–Fe(III)–OM nanoaggregates is amazing and needs attention. We infer that the unusual coordination environment of Fe(III), in which both As(V) and organic carbon protect its surface, helps in stabilizing Fe(III) in these coal samples, although further laboratory and field studies are needed to illuminate the conditions that facilitate the formation of such aggregates, preferably with direct imaging of the structure. Ferric Fe is also stabilized within ferritin, which is a hollow globular protein that holds a number of Fe nanoparticles within an internal cavity, and protects them from reaction. The Fe(III) in ferritin is considerably less reactive relative to free Fe(III) nanoparticles. For example, ferritin-encapsulated Fe(III) has a reduction potential as low as −300 mV at pH 7, much lower than the redox potentials needed to reduce isolated Fe(III) nanoparticles of a similar structure.[13] The enrichment of free HA adsorbed on Cr(III)–HA–Fe colloid surfaces has also been shown to contribute to its stability in a recent experimental study.[4] Thus, organo–mineral associations may effectively stabilize Fe(III) and As(V) in reducing environments such as anoxic sediments and peat, precursors of coal.

There are a few additional, possible reasons why Fe(III) and As(V) may be stabilized within ternary complexes of coal. First, the largely nonpolar organic matter surrounding the Fe(III) nanoparticles creates a stable low dielectric zone within the pocket, where ions that could reduce Fe(III) are unstable. The presence of large amounts of organic matter on the surface of Fe(III) minerals in these coal samples also can restrict access of the minerals to microorganisms, thus preventing enzymatic reduction of Fe(III) and associated As(V), although this kinetic effect may be less important over geological time. Further, like the stability of ferritin, the stability of the ternary complex may be a result of the stability of the organic matter conformation conferred by binding to the Fe(III), and possibly the effects of As(V) sorption on surface charge or bridging between particles. Lastly, plants and their litter layers are important sources of organic matter in Guizhou and other coal samples.[36] Due to oxygen transport by plants to their roots, not only root Fe(III) plaque is abundant, but also As(V), MMA and DMA, which are found to be associated with plant roots, even though As(III) is more abundant in reducing soils.[61–63] Therefore, it is plausible that these As(V) species in Guizhou coal samples may have originated from Fe(III)-plaque abundant in plant roots, and subsequently preserved by As(V)–Fe(III)–OM against reduction throughout the coalification process (see the Graphical Abstract).

3.7 Implications for As and Fe mobility in reducing environments

It is well known that the geochemical behavior of As is largely controlled by iron minerals, which are ubiquitous on earth and sensitive to redox processes.[13] The reductive dissolution of Fe minerals is considered as one of the most important ways for As to be released from aquifer sediments to groundwater.[64,65] Increasingly, studies have begun to investigate how natural organic matter (NOM) interacts with Fe and As, with aqueous and solid phase As–Fe–NOM complexes detected in reducing groundwater[66] and peat[58] and with enhanced preservation of organic matter observed also in reducing marine sediments.[9] A laboratory study found that the C/(C + Fe) ratios dominated the structural compositions and stabilities of Fe–NOM coprecipitates, suggesting that such coprecipitates, with Fe mainly as ferrihydrite, likely increase the resistance of organic matter to microbial decomposition/reduction.[16] A subsequent laboratory study confirmed that carbon-rich ferrihydrite polygalacturonic acid-coprecipitates and natural Fe-rich organic flocs contained nanosized clusters of lepidocrocite.[67] In wetlands, Guénet *et al.*[7] demonstrated by XAS that nano-lepidocrocite and small Fe clusters bound to NOM existed in wetland soils and the formation of small Fe clusters led to an increased ability for As adsorption. EXAFS studies of U.S. coal samples from Beulah–Zap, Wyodak–Anderson, and Lewiston–Stockton have shown significant amounts of Fe(III) in the coal samples, although the role of organic matter was not examined, nor the role of trace elements in Fe(III) stabilization.[68] As shown in this study, stabilization of ternary nano-sized arsenate–iron(III) oxyhydroxide–organic matter is possible in coal over geological time scales, and it begs the question on whether such nanoaggregates with oxidized forms of Fe and As with OM exist in much broader ranges of reduced, organic rich sedimentary environments, and in turn, make Fe and As less mobile.

4. Conclusions

While sulfuric As and reduced Fe species are common in coal samples worldwide, analyses of the local structures of Fe and As in five representative high-As coal samples from Guizhou by X-ray absorption spectroscopy suggest a new mode of occurrence as stable arsenate–iron(III) oxyhydroxide–organic matter nanoaggregates. Although this "As(V)–Fe(III)–OM" nanoaggregate system has been observed in laboratory experiments, its occurrence has rarely been reported in natural environments. These As(V)–Fe(III)–OM nanoaggregates in the coal samples likely originate from plant roots, and are preserved throughout the coalification process over a geological time scale. Nano-scale structural protection mechanisms of how metals and metalloids interact with organic matter to result in thermodynamic disequilibrium in

a broad range of reducing environments deserve more attention.

Conflicts of interest

There are no conflicts to declare.

Acknowledgements

Funding for this work was provided by the National Natural Science Foundation of China (Grant # 41831279, 41772265, and U1612442), the US National Science Foundation (NSF) grant EAR 15-21356, and the US National Institute of Environmental Health Sciences grant ES010349. Synchrotron data collection was supported by the Beijing Synchrotron Radiation Facility and Stanford Synchrotron Radiation Lightsource. Use of the Stanford Synchrotron Radiation Lightsource, SLAC National Accelerator Laboratory, is supported by the U.S. Department of Energy, Office of Science, Office of Basic Energy Sciences under Contract No. DE-AC02-76SF00515. We thank Drs. Robert B. Finkelman, Baoshan Zheng, Lirong Zheng and Zhenhua Ding for constructive discussions.

Notes and references

1 D. Vantelon, M. Davranche, R. Marsac, C. La Fontaine, H. Guénet, J. Jestin, G. Campaore, A. Beauvois and V. Briois, Iron speciation in iron–organic matter nanoaggregates: a kinetic approach coupling Quick-EXAFS and MCR-ALS chemometrics, *Environ. Sci.: Nano*, 2019, **6**, 2641–2651.

2 J. Ma, H. Guo, L. Weng, Y. Li, M. Lei and Y. Chen, Distinct effect of humic acid on ferrihydrite colloid-facilitated transport of arsenic in saturated media at different pH, *Chemosphere*, 2018, **212**, 794–801.

3 H. Guénet, M. Davranche, D. Vantelon, J. Gigault, S. Prévost, O. Taché, S. Jaksch, M. Pédrot, V. Dorcet, A. Boutier and J. Jestin, Characterization of iron–organic matter nano-aggregate networks through a combination of SAXS/SANS and XAS analyses: impact on As binding, *Environ. Sci.: Nano*, 2017, **4**, 938–954.

4 P. Liao, C. Pan, W. Ding, W. Li, S. Yuan, J. D. Fortner and D. E. Giammar, Formation and Transport of Cr(III)-NOM-Fe Colloids upon Reaction of Cr(VI) with NOM-Fe(II) Colloids at Anoxic–Oxic Interfaces, *Environ. Sci. Technol.*, 2020, **54**, 4256–4266.

5 X. Han, E. J. Tomaszewski, J. Sorwat, Y. Pan, A. Kappler and J. M. Byrne, Effect of Microbial Biomass and Humic Acids on Abiotic and Biotic Magnetite Formation, *Environ. Sci. Technol.*, 2020, **54**, 4121–4130.

6 Y. Lu, S. Hu, Z. Wang, Y. Ding, G. Lu, Z. Lin, Z. Dang and Z. Shi, Ferrihydrite transformation under the impact of humic acid and Pb: Kinetics, nano-scale mechanisms, and implications for C and Pb dynamics, *Environ. Sci.: Nano*, 2019, **6**, 747–762.

7 H. Guénet, M. Davranche, D. Vantelon, M. Pédrot, M. Al-Sid-Cheikh, A. Dia and J. Jestin, Evidence of organic matter control on As oxidation by iron oxides in riparian wetlands, *Chem. Geol.*, 2016, **439**, 161–172.

8 O. S. Pokrovsky, R. M. Manasypov, S. V. Loiko and L. S. Shirokova, Organic and organo-mineral colloids in discontinuous permafrost zone, *Geochim. Cosmochim. Acta*, 2016, **188**, 1–20.

9 W.-W. Ma, M.-X. Zhu, G.-P. Yang and T. Li, Iron geochemistry and organic carbon preservation by iron (oxyhydr)oxides in surface sediments of the East China Sea and the south Yellow Sea, *J. Mar. Syst.*, 2018, **178**, 62–74.

10 J. Kus, Application of confocal laser-scanning microscopy (CLSM) to autofluorescent organic and mineral matter in peat, coals and siliciclastic sedimentary rocks — A qualitative approach, *Int. J. Coal Geol.*, 2015, **137**, 1–18.

11 L. K. ThomasArrigo, C. Mikutta, J. Byrne, K. Barmettler, A. Kappler and R. Kretzschmar, Iron and Arsenic Speciation and Distribution in Organic Flocs from Streambeds of an Arsenic-Enriched Peatland, *Environ. Sci. Technol.*, 2014, **48**, 13218–13228.

12 J. M. Plach, A. V. C. Elliott, I. G. Droppo and L. A. Warren, Physical and Ecological Controls on Freshwater Floc Trace Metal Dynamics, *Environ. Sci. Technol.*, 2011, **45**, 2157–2164.

13 T. Borch, R. Kretzschmar, A. Kappler, P. V. Cappellen, M. Ginder-Vogel, A. Voegelin and K. Campbell, Biogeochemical Redox Processes and their Impact on Contaminant Dynamics, *Environ. Sci. Technol.*, 2010, **44**, 15–23.

14 C. Mikutta and R. Kretzschmar, Spectroscopic evidence for ternary complex formation between arsenate and ferric iron complexes of humic substances, *Environ. Sci. Technol.*, 2011, **45**, 9550–9557.

15 M. Hoffmann, C. Mikutta and R. Kretzschmar, Arsenite binding to natural organic matter: spectroscopic evidence for ligand exchange and ternary complex formation, *Environ. Sci. Technol.*, 2013, **47**, 12165.

16 K. Y. Chen, T. Y. Chen, Y. T. Chan, C. Y. Cheng, Y. M. Tzou, Y. T. Liu and H. Y. Teah, Stabilization of Natural Organic Matter by Short-Range-Order Iron Hydroxides, *Environ. Sci. Technol.*, 2016, **50**, 12612–12620.

17 A. Sundman, T. Karlsson, S. Sjöberg and P. Persson, Complexation and precipitation reactions in the ternary As(V)–Fe(III)–OM (organic matter) system, *Geochim. Cosmochim. Acta*, 2014, **145**, 297–314.

18 L. F. O. Silva, D. Pinto and B. D. Lima, Implications of iron nanoparticles in spontaneous coal combustion and the effects on climatic variables, *Chemosphere*, 2020, **254**, 126814.

19 R. B. Finkelman and L. Tian, The health impacts of coal use in China, *Int. Geol. Rev.*, 2018, **60**, 579–589.

20 Z. Hu and S. Gao, Upper crustal abundances of trace elements: A revision and update, *Chem. Geol.*, 2008, **253**, 205–221.

21 Y. Kang, G. Liu, C. L. Chou, M. H. Wong, L. Zheng and R. Ding, Arsenic in Chinese coals: distribution, modes of occurrence, and environmental effects, *Sci. Total Environ.*, 2011, **412-413**, 1–13.

22 K. M. Campbell and D. K. Nordstrom, Arsenic Speciation and Sorption in Natural Environments, *Rev. Mineral. Geochem.*, 2014, **79**, 185–216.

23 S. Dai, D. Ren, C. L. Chou, R. B. Finkelman, V. V. Seredin and Y. Zhou, Geochemistry of trace elements in Chinese coals: A review of abundances, genetic types, impacts on human health, and industrial utilization, *Int. J. Coal Geol.*, 2012, **94**, 3–21.
24 R. B. Finkelman, *Modes of Occurrence of Environmentally-Sensitive Trace Elements in Coal*, Springer Netherlands, 1995.
25 R. B. Finkelman, Modes of occurrence of potentially hazardous elements in coal: levels of confidence, *Fuel Process. Technol.*, 1994, **39**, 21–34.
26 X. Guo, C. Zheng, Y. Liu, J. Liu and X. Lu, The study on the mode of occurrence of mercury, arsenic and selenium in coal, *J. Eng. Thermophys.*, 2001, **22**, 763–766.
27 R. Finkelman, Modes of occurrence of trance elements in coal, US Geological Survey Open-File Report, 1981, pp. 81–99.
28 G. Liu, P. Yang, Z. Peng, G. Wang and Z. Cao, Occurrence of trace elements in coal of Yanzhou Mining District, *Geochim*, 2002, **31**, 85–90.
29 Y. E. Yudovich and M. P. Ketris, Arsenic in coal: a review, *Int. J. Coal Geol.*, 2005, **61**, 141–196.
30 H. E. Belkin, B. Zheng, D. Zhou and R. B. Finkelman, Preliminary results on the Geochemistry and Mineralogy of Arsenic in Mineralized Coals from Endemic Arsenosis areas in Guizhou Province, P.R. China, *Fourteenth Annual International Pittsburgh Coal Conference & Workshop*, 1997, vol. 23–27, pp. 1–20.
31 R. B. Finkelman, H. E. Belkin and B. Zheng, Health impacts of domestic coal use in China, *Proc. Natl. Acad. Sci. U. S. A.*, 1999, **96**, 3427–3431.
32 Z. Ding, B. Zheng, J. Zhang, H. E. Belkin, R. B. Finkelman, F. Zhao, D. Zhou, Y. Zhou and C. Chen, Preliminary study on the mode of occurrence of arsenic in high arsenic coals from southwest Guizhou Province, *Sci. China: Earth Sci.*, 1999, **42**, 655–661.
33 G. P. Huffman, F. E. Huggins, N. Shah and J. Zhao, Speciation of arsenic and chromium in coal and combustion ash by XAFS spectroscopy, *Fuel Process. Technol.*, 1994, **39**, 47–62.
34 T. Karlsson and P. Persson, Complexes with aquatic organic matter suppress hydrolysis and precipitation of Fe(III), *Chem. Geol.*, 2012, **322-323**, 19–27.
35 A. M. Vindedahl, J. H. Strehlau, W. A. Arnold and R. L. Penn, Organic Matter and Iron Oxide Nanoparticles: Aggregation, Interactions, and Reactivity, *Environ. Sci.: Nano*, 2016, **3**, 494–505.
36 Z. Ding, B. Zheng, J. Long, H. E. Belkin, R. B. Finkelman, C. Chen, D. Zhou and Y. Zhou, Geological and geochemical characteristics of high arsenic coals from endemic arsenosis areas in southwestern Guizhou Province, China, *Appl. Geochem.*, 2001, **16**, 1353–1360.
37 S. Dai and R. B. Finkelman, Coal geology in China: an overview, *Int. Geol. Rev.*, 2018, **60**, 531–534.
38 M. Sun, G. Liu, Q. Wu and W. Liu, Speciation analysis of inorganic arsenic in coal samples by microwave-assisted extraction and high performance liquid chromatography coupled to hydride generation atomic fluorescence spectrometry, *Talanta*, 2013, **106**, 8–13.
39 T. Kanduč, Z. Šlejkovec, N. Mori, M. Vrabec, T. Verbovšek, S. Jamnikar and M. Vrabec, Multielemental composition and arsenic speciation in low rank coal from the Velenje Basin, Slovenia, *J. Geochem. Explor.*, 2019, **200**, 284–300.
40 F. E. Huggins and G. P. Huffman, Modes of occurrence of trace elements in coal from XAFS spectroscopy, *Int. J. Coal Geol.*, 1996, **32**, 31–53.
41 Y. Zhang, S. Li, L. Zheng, J. Chen and Y. Zheng, Evaluation of arsenic sorption and mobility in stream sediment and hot spring deposit in three drainages of the Tibetan Plateau, *Appl. Geochem.*, 2017, **77**, 89–101.
42 Y. Meng, G. Gong, D. Wei, Y. Xie and Z. Yin, Comparative microstructure study of high strength alumina and bauxite insulator, *Ceram. Int.*, 2014, **40**, 10677–10684.
43 U. Schwertmann and R. M. Cornell, *Iron Oxides in the Laboratory: Preparation and Characterization*, Wiley, Weinheim, 2000.
44 J. Sun, B. J. Mailloux, S. N. Chillrud, A. van Geen, A. Thompson and B. C. Bostick, Simultaneously quantifying ferrihydrite and goethite in natural sediments using the method of standard additions with X-ray absorption spectroscopy, *Chem. Geol.*, 2018, **476**, 248–259.
45 B. C. Bostick, J. Sun, J. D. Landis and J. L. Clausen, Tungsten Speciation and Solubility in Munitions-Impacted Soils, *Environ. Sci. Technol.*, 2018, **52**, 1045–1053.
46 B. Ravel and M. Newville, ATHENA, ARTEMIS, HEPHAESTUS: data analysis for X-ray absorption spectroscopy using IFEFFIT, *J. Synchrotron Radiat.*, 2005, **12**, 537–541.
47 T. Ressler, WinXAS: a Program for X-ray Absorption Spectroscopy Data Analysis under MS-Windows, *J. Synchrotron Radiat.*, 1998, **5**, 118–122.
48 F. Huggins, F. Goodarzi and C. Lafferty, *Mode of Occurrence of Arsenic in Subbituminous Coals*, 1996.
49 A. Kolker, F. E. Huggins, C. A. Palmer, N. Shah, S. S. Crowley, G. P. Huffman and R. B. Finkelman, Mode of occurrence of arsenic in four US coals, *Fuel Process. Technol.*, 2000, **63**, 167–178.
50 A. Voegelin and S. J. Hug, Catalyzed oxidation of arsenic(III) by hydrogen peroxide on the surface of ferrihydrite: an in situ ATR FTIR study, *Environ. Sci. Technol.*, 2003, **37**, 972–978.
51 S. Fendorf, M. J. Eick, P. Grossl and D. L. Sparks, Arsenate and Chromate Retention Mechanisms on Goethite. 1. Surface Structure, *Environ. Sci. Technol.*, 1997, **31**, 315–320.
52 T. Ressler, J. Wong, J. Roos and I. L. Smith, Quantitative Speciation of Mn-Bearing Particulates Emitted from Autos Burning (Methylcyclopentadienyl)manganese Tricarbonyl-Added Gasolines Using XANES Spectroscopy, *Environ. Sci. Technol.*, 2000, **34**, 950–958.
53 W. P. Inskeep, R. E. Macur, G. Harrison, B. C. Bostick and S. Fendorf, Biomineralization of As(V)-hydrous ferric oxyhydroxide in microbial mats of an acid-sulfate-chloride geothermal spring, Yellowstone National Park 1, *Geochim. Cosmochim. Acta*, 2004, **68**, 3141–3155.

54 F. Vejahati, Z. Xu and R. Gupta, Trace elements in coal: Associations with coal and minerals and their behavior during coal utilization – A review, *Fuel*, 2010, **89**, 904–911.
55 K. W. Riley, D. H. French, O. P. Farrell, R. A. Wood and F. E. Huggins, Modes of occurrence of trace and minor elements in some Australian coals, *Int. J. Coal Geol.*, 2012, **94**, 214–224.
56 C.-L. Chou, Sulfur in coals: A review of geochemistry and origins, *Int. J. Coal Geol.*, 2012, **100**, 1–13.
57 A. C. Cismasu, F. M. Michel, A. P. Tcaciuc, T. Tyliszczak and J. G. E. Brown, Composition and structural aspects of naturally occurring ferrihydrite, *C. R. Geosci.*, 2011, **343**, 210–218.
58 P. Langner, C. Mikutta and R. Kretzschmar, Arsenic sequestration by organic sulphur in peat, *Nat. Geosci.*, 2012, **5**, 66–73.
59 C. Mikutta, J. Frommer, A. Voegelin, R. Kaegi and R. Kretzschmar, Effect of citrate on the local Fe coordination in ferrihydrite, arsenate binding, and ternary arsenate complex formation, *Geochim. Cosmochim. Acta*, 2010, **74**, 5574–5592.
60 C. Mikutta, X-ray absorption spectroscopy study on the effect of hydroxybenzoic acids on the formation and structure of ferrihydrite, *Geochim. Cosmochim. Acta*, 2011, **75**, 5122–5139.
61 T. Sarwar, S. Khan, S. Muhammad and S. Amin, Arsenic speciation, mechanisms, and factors affecting rice uptake and potential human health risk: A systematic review, *Environ. Technol. Innovation*, 2021, **22**, 101392.
62 A. I. González de las Torres, I. Giráldez, F. Martínez, P. Palencia, W. T. Corns and D. Sánchez-Rodas, Arsenic accumulation and speciation in strawberry plants exposed to inorganic arsenic enriched irrigation, *Food Chem.*, 2020, **315**, 126215.
63 J. M. Garnier, F. Travassac, V. Lenoble, J. Rose, Y. Zheng, M. S. Hossain, S. H. Chowdhury, A. K. Biswas, K. M. Ahmed, Z. Cheng and A. van Geen, Temporal variations in arsenic uptake by rice plants in Bangladesh: The role of iron plaque in paddy fields irrigated with groundwater, *Sci. Total Environ.*, 2010, **408**, 4185–4193.
64 Y. Zheng, M. Stute, A. van Geen, I. Gavrieli, R. Dhar, H. J. Simpson, P. Schlosser and K. M. Ahmed, Redox control of arsenic mobilization in Bangladesh groundwater, *Appl. Geochem.*, 2004, **19**, 201–214.
65 L. Rodríguez-Lado, G. Sun, M. Berg, Q. Zhang, H. Xue, Q. Zheng and C. A. Johnson, Groundwater arsenic contamination throughout China, *Science*, 2013, **341**, 866–868.
66 H. Guo, B. Zhang and Y. Zhang, Control of organic and iron colloids on arsenic partition and transport in high arsenic groundwaters in the Hetao basin, Inner Mongolia, *Appl. Geochem.*, 2011, **26**, 360–370.
67 L. K. ThomasArrigo, J. M. Byrne, A. Kappler and R. Kretzschmar, Impact of Organic Matter on Iron(II)-Catalyzed Mineral Transformations in Ferrihydrite–Organic Matter Coprecipitates, *Environ. Sci. Technol.*, 2018, **52**, 12316–12326.
68 S. R. Wasserman, R. E. Winans and R. McBeth, Iron Species in Argonne Premium Coal Samples: An Investigation Using X-ray Absorption Spectroscopy, *Energy Fuels*, 1996, **10**, 392–400.
69 W. P. Inskeep, R. E. Macur, G. Harrison, B. C. Bostick and S. Fendorf, Biomineralization of As(V)-hydrous ferric oxyhydroxide in microbial mats of an acid-sulfate-chloride geothermal spring, Yellowstone National Park, *Geochim. Cosmochim. Acta*, 2004, **68**, 3141–3155.

